

de Broglie Wave Phase Shifts Induced by Surfaces Closer than 25 nm

Alexander D. Cronin and John D. Perreault

Department of Physics, University of Arizona, 1118 E 4th St, Tucson, AZ 85721

E-mail: cronin@physics.arizona.edu

Abstract. Four atom optics experiments that each serve to measure atom-surface interactions near nanofabricated gratings are presented here. In these experiments atoms in a beam travel within 25 nm of a material grating bar, and the analysis incorporates phase shifts for the atomic de Broglie waves due to interactions between Na atoms and silicon nitride surfaces. One atom diffraction experiment determines the van der Waals coefficient $C_3 = 2.7 \pm 0.8 \text{ meVnm}^3$, and one atom interferometer experiment determines $C_3 = 4 \pm 1 \text{ meVnm}^3$. The results of all four experiments are consistent with the Lifshitz prediction that is explicitly calculated here for Na-silicon nitride to be $C_3 = 3.25 \text{ meVnm}^3$. The four atom optics experiments and review of van der Waals theory are complemented by similar experiments using electron beams and analysis of image-charge effects.

1. Introduction

Ten nm away from a surface the potential energy for an atom is approximately $3 \mu\text{eV}$, and for an electron it is about 10,000 times larger. More precisely, the van der Waals potential for sodium atoms and the image-charge potential for electrons both depend on the permittivity of the surface material; both potentials are also affected by surface charges, surface coatings, and surface geometry. Precise knowledge of the potential close to real surfaces is now needed for understanding atom optics experiments and nanotechnology devices, yet measurements of atom-surface interaction strengths have only been made for a few systems so far. Here we present four atom optics experiments that serve to measure the potential energy for atoms due to a surface located within 25 nm. Comparison to theoretical values of the non-retarded atom-surface van der Waals interaction will be made in the discussion.

Our experiments are based on coherent transmission of sodium atom de Broglie waves through an array of 50 nm wide channels in a silicon nitride nanostructure grating. Transmitted atoms pass within 25 nm to a grating bar surface, and remain this close for only 10^{-10} sec. Even in this short time, interactions with the channel walls modify the phase of the atom waves. Phase front curvature on the nanometer scale has the observed effect of modifying the phase Φ_n and amplitude $|A_n|$ in each far-field diffraction order. We measured atom diffraction intensities and atom interferometer fringe phase shifts in order to determine the potential for sodium atoms induced by surfaces of silicon nitride.

For comparison we used the same nanostructure gratings to diffract electron beams. Despite the 10,000 times larger potential energy (at 10 nm) due to image-charge effects, electron diffraction shows similar features to atom diffraction as a result of stronger interactions with the surface over shorter time scales.

2. Nanostructure Gratings

The 100-nm period gratings were fabricated by T.A. Savas at MIT using photolithography with standing waves of UV laser light. The etch procedures used to create the silicon nitride nanostructures are described in [1]. The bars are free-standing trapezoidal columns and their dimensions have been measured to an accuracy of 1.5 nm using scanning electron microscope (SEM) images such as those shown in Figures 1 and 2.

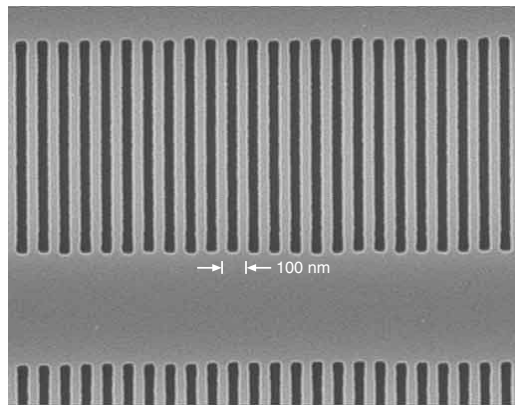


Figure 1. Front view of a nanostructure grating with a 100-nm period. The free-standing silicon nitride bars appear light in this image. Image courtesy of T.A. Savas at the MIT NanoStructures Laboratory.

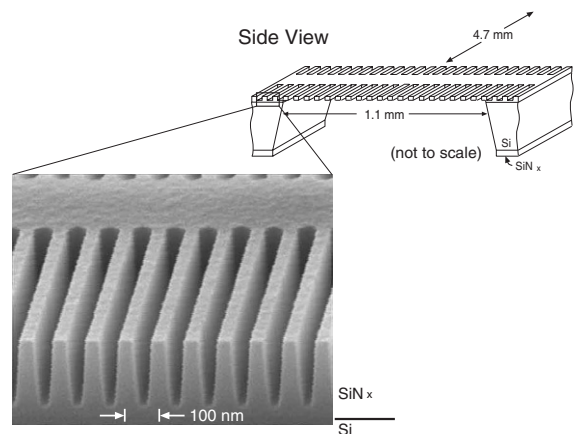


Figure 2. Cross-section of a cleaved grating. Note the trapezoidal bar profile. Bars in this region are not free standing, but are attached to a substrate. Image courtesy of T.A. Savas.

To understand how van der Waals interactions modify the amplitude and phase of diffracted atom waves, we consider three steps. First, a model for the potential in all space around the grating bars is needed. Second, the phase shift and absorption for atom waves transmitted through this potential is calculated as a function of position. Finally, the propagation to the far-field is given by a Fourier transform of the transmission function.

To begin, we approximate the potential in each channel by a sum of van der Waals potentials for an atom and two infinite planes,

$$V(r) = -C_3 \left(\frac{1}{r_1^3} + \frac{1}{r_2^3} \right) \quad (1)$$

where r_1 and r_2 are the distances along the normals to the walls of the channel, and r will be defined in terms of the coordinates ξ and z . Because of the trapezoidal shape of the bars, the channel walls are not parallel. We also considered the potential due to a sum of uncorrelated atom-atom interactions between a beam atom and all the atoms that compose the grating. The potential energy landscape calculated this way is shown in Figure 3 and the marginal validity of this approach will be discussed later.

The phase shift for atom waves transmitted through the channel can be computed in the WKB approximation,

$$\phi(\xi) = \int \sqrt{\frac{2m}{\hbar^2} [E - V(\xi, z)]} dz \quad (2)$$

where m is the atomic mass, E is the total atomic energy, and $V(\xi, z)$ is the van der Waals potential energy. The coordinate axes ξ and z are defined in Figures 3 and 4. Curved wave fronts due to $\phi(\xi)$ are shown in Figure 4 given a plane wave incident on the gratings. With

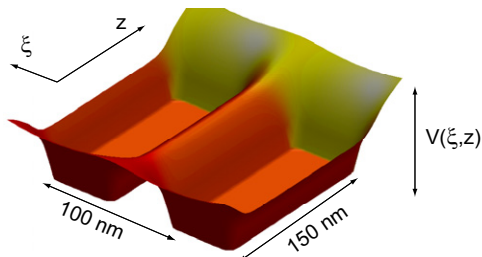


Figure 3. The potential energy $V(\xi, z)$ in the vicinity of trapezoidal columns can be approximated by a pairwise interaction. The vertical axis is shown on a log scale.

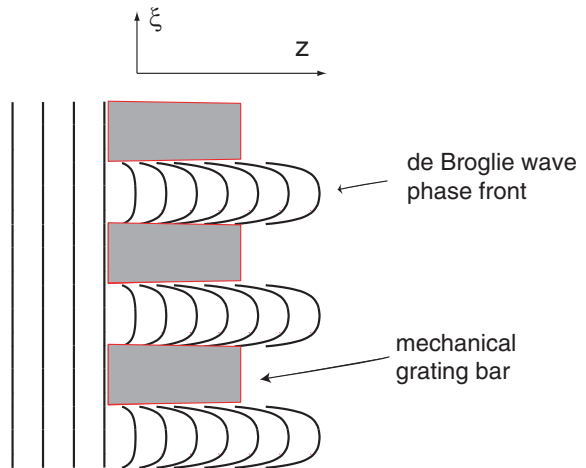


Figure 4. Modified wave fronts with $\phi(\xi)$ due to $V(\xi, z)$ calculated by Eqs. 1 and 2.

this model of the grating windows as phase masks, the wave function after the grating has an additional phase factor that depends on transverse position within each window given by

$$T(\xi) = \text{rect}\left(\frac{\xi}{w}\right) e^{i\phi(\xi)}, \quad (3)$$

where $T()$ is the transmission function, ξ is measured from the center of each window and $\text{rect}()$ describes the absorption from the grating bars. Then the wave function at the detector plane is a sum of diffraction orders

$$\psi(x) = \sum_n |A_n| e^{i\Phi_n} L(x - x_n) \quad (4)$$

with

$$|A_n| e^{i\Phi_n} = \int_{-w/2}^{w/2} T(\xi) d\xi = \int_{-w/2}^{w/2} e^{i\phi(\xi) + ink_g \xi} d\xi \quad (5)$$

where $k_g = 2\pi/d$ is the grating wavenumber, w is the size of each window between the grating bars, and $L(x)$ is the line shape of the atom beam in the detector plane, and x_n is the displacement of the n th diffraction order given by $x_n = z_{det} n \lambda_{dB}/d$. In our experiment $z_{det} = 2.4$ m, $d = 100$ nm, and λ_{dB} can range from 270 pm (for 600 m/s Na atoms) to 54 pm (for 3000 m/s Na atoms). More formal derivations of $\psi(x)$ are given in [2, 3] from our group and in [4, 5] from the Toennies group which uses a slightly different description of the atom optics theory.

The phase (Φ_n) and amplitude ($|A_n|$) of each diffraction order are both functions of the potential strength (C_3), the atom velocity (v), grating window size (w), grating period (d), grating thickness (t), and grating bar wedge angle (α). For typical values ($v = 2000$ m/s, $w = 55$ nm, $d = 100$ nm, $t = 150$ nm, and $\alpha = 5^\circ$) theoretical plots of $|A_n(C_3)|$ and $\Phi_n(C_3)$ are shown in Figures 5 and 6.

3. Atom and Electron Diffraction Experiments

Diffraction data displayed in Figure 7 permit us to measure the intensities $|A_n|^2$ and the mean atom beam velocity, as well as the velocity distribution. When combined with SEM measurements of the grating geometry, a single diffraction pattern is sufficient to determine C_3 , because the values of $|A_n|^2$ depend on C_3 as shown in Eqs. 1, 2 and 5.

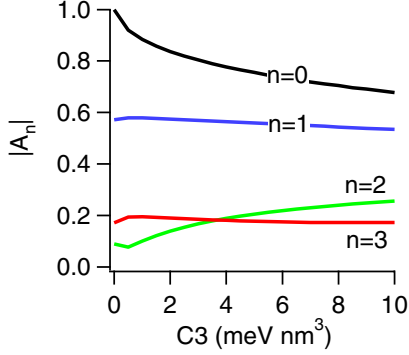


Figure 5. Diffraction amplitudes $|A_n|$ depend on C_3 . The prediction includes fixed parameters ($v = 2000$ m/s, $w = 55$ nm, $d = 100$ nm, $t = 150$ nm, and $\alpha = 5^\circ$).

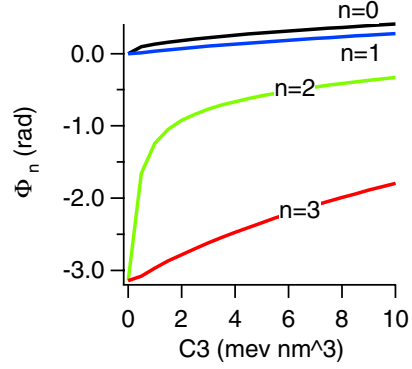


Figure 6. Phases Φ_n for each diffraction order depend on C_3 . The prediction includes fixed parameters ($v = 2000$ m/s, $w = 55$ nm, $d = 100$ nm, $t = 150$ nm, and $\alpha = 5^\circ$).

Ideally, we would like to manipulate C_3 and verify experimentally that this changes $|A_n|$. Instead, we studied how each $|A_n|$ for $n=(0$ to $5)$ depends on atomic velocity. For example, Figures 7 and 8 show different diffraction intensities ($|A_n|^2$) for two different velocity Na beams. As expected, the diffraction angle changes too, and this permits us to measure v . To first order in $V(r)/E$ the parameters $C_3 t/v$ are grouped together in $\phi(\xi)$ and therefore $|A_n|$ are affected in a similar way by changing v or C_3 . This experiment is described in [3].

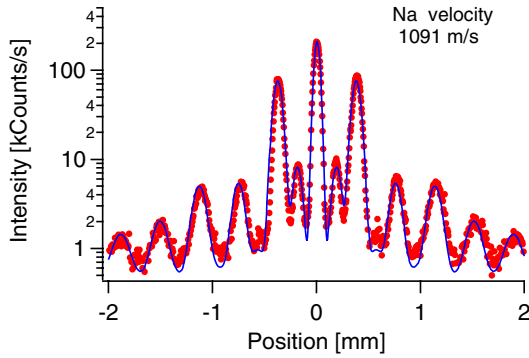


Figure 7. Sodium atom (and molecule) diffraction data using a supersonic beam seeded with Ar carrier gas to provide mean velocity of 1091 m/s.

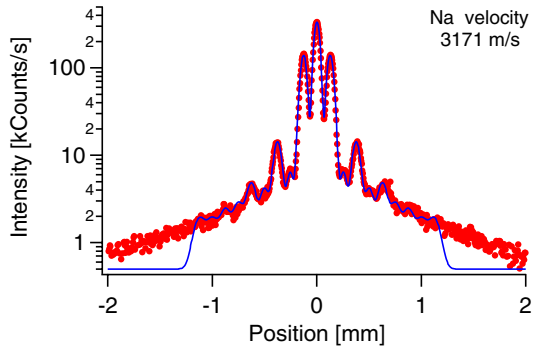


Figure 8. Sodium atom (and molecule) diffraction data using a supersonic beam seeded with He carrier gas to provide mean velocity of 3171 m/s.

We emphasize here that if $C_3 = 0$, the nano structure would be purely an absorbing grating, and the $|A_n|$ would not change with atom velocity. It is the van der Waals interaction that gives the gratings a complex transmission function, and makes $|A_n|$ depend on incident atom velocity. With least squared fits to $|A_n|$ we determined $C_3 = 2.7 \pm 0.8$ meVnm³. We also verified using χ^2 that the $1/r^3$ form of the potential gives the best fit to the data.

In our second experiment we observed how the intensities $|A_n|^2$ vary when the grating is rotated as shown in Figures 9 and 10 and described in [2]. Due to the thickness of the grating bars the angle of incidence affects the projected open fraction. If $C_3 = 0$ then twisting the grating would cause missing diffraction orders when the projected open fraction is $\frac{1}{2}$, or $\frac{1}{3}$ as

shown with dashed lines in Figure 10. However, a better fit to the data is obtained using the theory for $|A_n|$ described in [2] (similar to Eq. 5) with $C_3 = 5 \text{ meVnm}^3$. This produces the solid lines in Figure 10. We also observe asymmetric diffraction patterns, i.e. *blazed* diffraction, in this experiment, and our model reproduces this result. Asymmetric phase profiles $\phi(\xi)$ for de Broglie waves transmitted through each window are provided by a combination of three ingredients: non-normal incidence, trapezoidal bar shape, and non-zero C_3 . We observe even more asymmetric diffraction patterns with electron beams as discussed next.

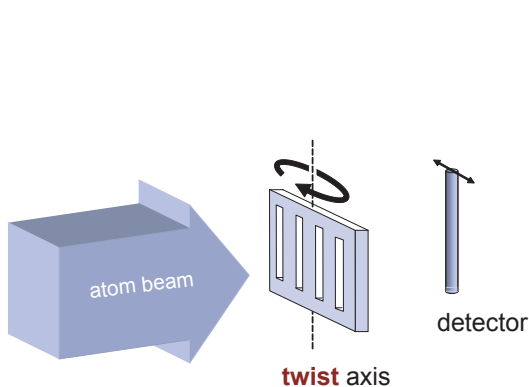


Figure 9. Geometry of the diffraction experiments. In [3] the beam velocity is changed. In [2] the grating is rotated.

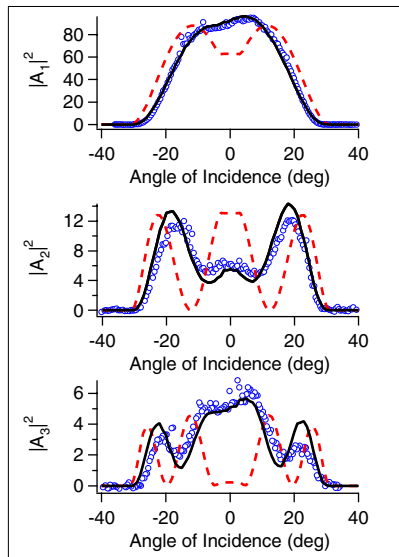


Figure 10. The intensity in the first three diffraction orders ($|A_1|^2$, $|A_2|^2$, and $|A_3|^2$) as a function of the angle of incidence.

We found that electron diffraction with nanostructure gratings is also affected by the surfaces as far as 20 nm away, similar to the way van der Waals interactions modify atom diffraction. To keep the grating bars from getting charged by the electron beam we coated them with 1 nm of gold. Near this gold-coated silicon nitride surface, electrons have an electrostatic potential energy that we calculate from the method of images to be

$$V(r) = -e^2 \left(\frac{1}{2r_1} + \frac{1}{2r_2} \right) \left(\frac{\epsilon - 1}{\epsilon + 1} \right) \quad (6)$$

in Gaussian units, where ϵ is the ratio of the dielectric permittivity compared to that of free space and e is the charge of the electron and as before, r_1 is the distance to one wall. Using this image-charge potential we calculated the phase shift $\phi(\xi)$ and thus the diffraction amplitudes $|A_n|$ for electrons. Figure 11 shows electron diffraction data and a theoretical diffraction pattern based on Equations 2, 5, and 6, using best fit parameters $\epsilon = 4$, and an angle of incidence 5 degrees. Note that if the image-charge effect were not included then the model for $|A_n|^2$ in Figure 11 would be symmetric about the zeroth order.

Twenty nm away from this surface the potential for electrons is 0.02 eV as compared to the atom-wall potential of $0.4 \mu\text{eV}$. This is 50,000 times larger for electrons than for sodium atoms. However, the phase shift $\phi(\xi)$ near $\xi = 20 \text{ nm}$ is similar for electrons and atoms because the velocity of 500 eV electrons (13,000 km/s) is four orders of magnitude larger than that for 0.12 eV sodium atoms (1 km/s).

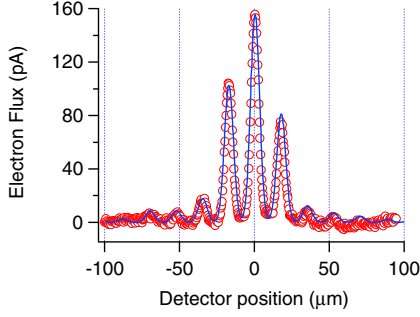


Figure 11. Electron diffraction from a beam transmitted through a nanostructure grating. The theoretical curve includes the effect of the image-charge on the diffraction intensities $|A_n|^2$.

4. Atom Interferometer Experiments

In addition to the diffraction amplitudes $|A_n|$, there are diffraction phases Φ_n in each order. We measured the phase shift in the zeroth order (Φ_0) due to transmission through a removable interaction grating (IG) with an interferometer [6]. The geometry of this experiment is shown in Figure 12, and permits us to study the interference fringes as a function of the IG position. Interference fringe data are shown in Figure 13 for the cases of the IG obscuring either path I, path II, or neither. The directly measured phase shift, $\Phi_{meas} = 0.22 \pm 0.02$ radians, is consistent with $C_3 = 4 \pm 1$ meVnm³. A more detailed discussion of how to determine Φ_0 and C_3 from the measured phase shift is given in a separate entry of the CAMS conference proceedings by J.D. Perreault and in reference [6].

We also measured the phase difference $\Phi_2 - \Phi_1 = 0.6 \pm 0.4$ radians, by comparing the relative phases of four separate interferometers formed by adjacent pairs of the $n = (-2, -1, 0, 1, 2)$ diffraction orders of the first interferometer grating. This phase difference can be compared to that predicted in Figure 6 and is consistent with $C_3 = 4$ meVnm³.

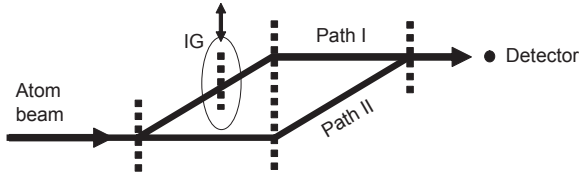


Figure 12. Top view of the atom interferometer. Three gratings make the interferometer and a removable interaction grating (IG) is used in [6] to study the phase shift Φ_0 caused by the van der Waals interaction.

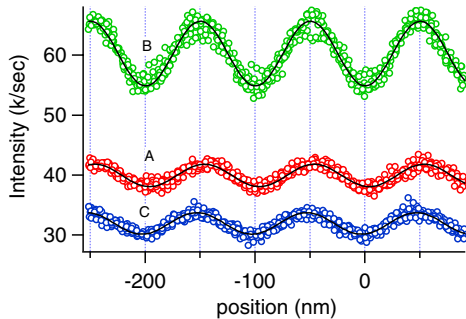


Figure 13. Atom interference fringe data for three cases: (A) interaction grating (IG) located in path I, (B) no IG, (C) IG in path II of the atom interferometer.

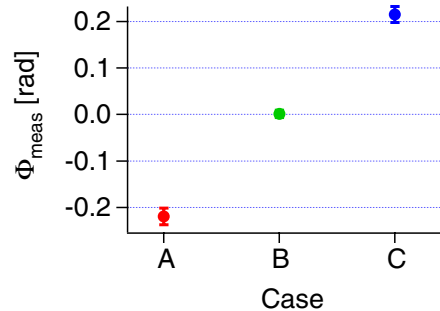


Figure 14. Best fit phase and statistical error bars for the three cases: (A) IG in path I, (B) IG removed, (C) IG in path II of the interferometer.

5. Discussion

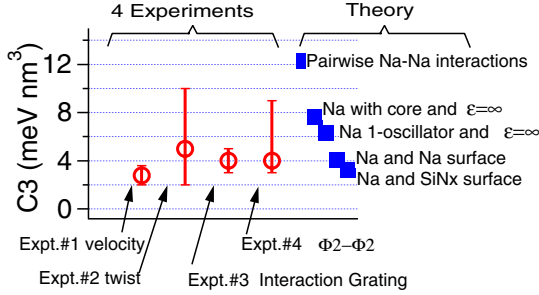


Figure 15. Comparison of C_3 values determined by the four experiments presented here (red circles). Theoretical predictions based on different descriptions of the atom and the surface are shown (blue squares).

To compare our measurements with theory, we reviewed calculations of C_3 for sodium atoms and various surfaces as shown in Figure 15. The Lifshitz formula [7] for C_3 is

$$C_3 = \frac{\hbar}{4\pi} \int_0^\infty \alpha(i\omega) \frac{\epsilon(i\omega) - 1}{\epsilon(i\omega) + 1} d\omega \quad (7)$$

where $\alpha(i\omega)$ is the polarizability of the atom and $\epsilon(i\omega)$ is the permittivity of the surface. For a perfect conductor ($\epsilon=\infty$) and sodium atoms, Derevianko *et al.* [8] calculated $C_3 = 7.60 \text{ meVnm}^3$ and noted that 16% of this value is due to the core electrons. A single Lorentz oscillator model for an atom with no damping gives the polarizability:

$$\alpha(i\omega) = \frac{\alpha(0)}{1 + (\frac{\omega}{\omega_0})^2}. \quad (8)$$

For sodium atoms $\alpha(0) = 0.0241 \text{ nm}^3$ [9] and $\omega_0 = 2\pi c/(590 \text{ nm})$. Combining this with ($\epsilon=\infty$) in Eq. 7 gives $C_3 = \hbar\omega_0\alpha(0)/8 = 6.3 \text{ meVnm}^3$. This agrees with the non-retarded limit in [10].

For a metal surface, the Drude model describes $\epsilon(i\omega)$ with the plasma frequency and damping:

$$\epsilon(i\omega) = 1 + \frac{\omega_p^2}{\omega(\omega + \gamma)}. \quad (9)$$

For sodium metal, $\hbar\omega_p = 5.8 \text{ eV}$ and $\hbar\gamma = 23 \text{ meV}$, resulting in $C_3 = 4.1 \text{ meV nm}^3$ for a sodium atom and a bulk sodium surface. For an insulating surface Bruhl *et al* [5] used a model with

$$\epsilon(i\omega) = \frac{\omega^2 + (1 + g_0)\omega_0^2}{\omega^2 + (1 - g_0)\omega_0^2} \quad (10)$$

and $\hbar\omega_0 \equiv E_s = 13 \text{ eV}$ and $g_0 = 0.588$ for silicon nitride. Using this expression and the one-oscillator model for sodium atoms yields $C_3 = 3.25 \text{ meVnm}^3$.

The pairwise sum of atom-atom interactions for sodium atoms near bulk sodium metal gives

$$V(x) = -N \int_x^\infty \int_{-\infty}^\infty \int_{-\infty}^\infty \frac{C_6}{r^6} dy' dz' dx' = -\frac{\pi N C_6}{6x^3} \quad (11)$$

where x is the atom-surface distance. Using the London result for $C_6 = (3/4)\hbar\omega_0\alpha(0)^2$ [11] and the number density of bulk sodium for N gives a value for $C_3 = 12.3 \text{ meVnm}^3$ (also, if N is replaced by $\alpha(0)^{-1}$, this calculation gives $C_3 = \pi\hbar\omega_0\alpha(0)/8 = 19.6 \text{ meVnm}^3$). The value using the pairwise sum is three times larger than the value (4.1 meVnm^3) obtained for the same atom-surface system using Eqs.7, 8, and 9. The different values obtained with these two approaches

demonstrate the non-additivity of the van der Waals potential. Our measurements of C_3 are all much closer to the Lifshitz result.

One example of how van der Waals forces influence atom optics with nanotechnology is that the figure of merit for an interferometer discussed in [12] ($\text{FOM} = \text{contrast} \times \sqrt{I/I_{inc}}$) depends on C_3 . Here we show that to maximize the FOM, different open fractions need to be chosen if $C_3 \neq 0$, especially for slower atom beams as shown in Figure 16.

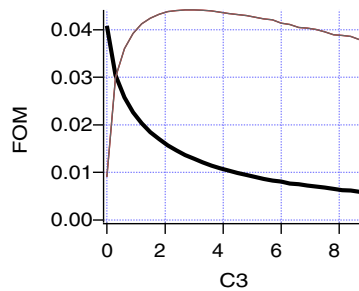


Figure 16. The FOM depends on C_3 . The thick curve is for windows ($w_1=56$, $w_2=50$, $w_3=37$ nm) that maximize the FOM if $C_3 = 0$. The thin curve is for windows ($w_1=93$, $w_2=88$, $w_3=37$ nm) that maximize the FOM for $C_3 = 3$ meVnm³. These calculations are for Na atoms with $v = 100$ m/s.

6. Conclusion

We used nanostructure gratings with 50-nm wide channels between free-standing bars in four experiments to measure the strength of atom-surface interactions. We detected phase shifts and intensity changes for atom beams that we attribute to van der Waals interactions with the walls of a nanostructure grating. A model based on complex transmission functions for de Broglie wave optics can explain both atom and electron diffraction patterns.

Acknowledgments

This research was supported by a Research Innovation Award from the Research Corporation and by National Science Foundation Grants No.0354947 and ECS-0404350. We thank Tim Savas for making the gratings and Ben McMorran for analyzing electron diffraction.

References

- [1] T. A. Savas, M. L. Schattenburg, J. M. Carter, and H. I. Smith. Large-area achromatic interferometric lithography for 100 nm period gratings and grids. *J. Vac. Sci. Tech. B*, 14(6):4167, 1996.
- [2] A. D. Cronin and J. D. Perreault. Phasor analysis of atom diffraction from a rotated material grating. *Phys. Rev. A*, 70(4):043607, 2004.
- [3] J. D. Perreault, A. D. Cronin, and T. Savas. Using atomic diffraction of Na from material gratings to measure atom-surface interactions. *Phys. Rev. A*, 71(5):053612, 2005.
- [4] R. E. Grisenti, W. Schollkopf, J. P. Toennies, G. Hegerfeldt, T. Kohler. Determination of atom-surface van der Waals potentials from transmission-grating diffraction intensities. *Phys. Rev. Lett.*, 83(9):1755, 1999.
- [5] R. Bruhl, P. Fouquet, R. E. Grisenti, J. P. Toennies, G. C. Hegerfeldt, T. Kohler, M. Stoll, and D. Walter. The van der Waals potential between metastable atoms and solid surfaces: Novel diffraction experiments vs theory. *Europhys. Lett.*, 59(3):357, 2002.
- [6] J. D. Perreault and A. D. Cronin. Observation of atom wave phase shifts induced by van der Waals atom-surface interactions. *arXiv:physics/0505160*, 2005.
- [7] E. M. Lifshitz. *Sov. Phys. JETP*, 2:73, 1956.
- [8] A. Derevianko, W. R. Johnson, M. S. Safranov, and J. F. Baab. High precision calculations of dispersion coefficients, static dipole polarizabilities, and atom-wall interaction constants for alkali-metal atoms. *Phys. Rev. Lett.*, 82:3589, 1999.
- [9] C. R. Ekstrom, J. Schmiedmayer, M. S. Chapman, T. D. Hammond, and D. E. Pritchard. Measurement of the electric polarizability of sodium with an atom interferometer. *Phys. Rev. A*, 51:3883, 1995.
- [10] M. Marinescu, A. Dalgarno, and J. F. Baab. Retarded long-range potentials for the alkali-metal atoms and a perfectly conducting wall. *Phys. Rev. A*, 55:1530, 1997.
- [11] P.W. Milonni *The Quantum Vacuum*. Academic Press, 1994.
- [12] P. R. Berman, editor. *Atom Interferometry*. Academic Press, 1997.